

CONSTRAINING THE REDSHIFT $Z \sim 6$ QUASAR LUMINOSITY FUNCTION USING GRAVITATIONAL LENSING

JULIA M. COMERFORD, ZOLTÁN HAIMAN¹
Princeton University Observatory, Princeton, NJ 08544, USA
comerfrd@astro.princeton.edu, zoltan@astro.princeton.edu

JOOP SCHAYE
Institute for Advanced Study, School of Natural Sciences, Olden Lane, Princeton, NJ 08540, USA
schaye@ias.edu

Submitted to The Astrophysical Journal

ABSTRACT

Recent discoveries by the Sloan Digital Sky Survey (SDSS) of four bright $z \sim 6$ quasars could constrain the mechanism by which the supermassive black holes powering these sources are assembled. Here we compute the probability that the fluxes of the quasars are strongly amplified by gravitational lensing, and therefore the likelihood that the black hole masses are overestimated when they are inferred assuming Eddington luminosities. The poorly-constrained shape of the intrinsic quasar luminosity function (LF) at redshift ~ 6 results in a large range of possible lensing probabilities. If the LF is either steep, or extends to faint magnitudes, the probability for amplification by a factor $\mu \gtrsim 10$ (and with only one image detectable by SDSS) can reach essentially 100%. We show that future observations, in particular, either of the current four quasars at the high angular resolution provided by the Hubble Space Telescope, or of an increased sample of ~ 20 redshift six quasars at the current angular resolution, should either discover several gravitational lenses, or else provide interesting new constraints on the shape of the $z \sim 6$ quasar LF.

Subject headings: cosmology: observations — cosmology: theory — galaxies: high-redshift — gravitational lensing — quasars: general — black hole physics

1. INTRODUCTION

The Sloan Digital Sky Survey (SDSS) has recently discovered several extremely bright and distant quasars with redshifts $z \sim 6$, whose luminosities are a result of gas accretion onto supermassive black holes (BHs). These rare objects have luminosities at the far bright tail of the quasar luminosity function (LF), corresponding to $\sim 5\sigma$ peaks in the density field in models in which quasars populate dark matter halos (Haiman & Loeb 2001; Fan et al. 2001b). By assuming that the observed luminosities equal the limiting Eddington luminosities of the BHs, the masses of all these BHs are inferred to be a few $\times 10^9 M_\odot$. The mere existence of such massive BHs at so early a stage in the evolution of the universe should provide insight into the formation and growth of supermassive black holes (Haiman & Loeb 2001).

The above estimates for the masses of the BHs associated with the SDSS quasars scale directly with the inferred luminosities, and thus with the observed fluxes of the quasars. However, the apparent fluxes can be increased by gravitational lensing. If a quasar is gravitationally lensed and this is not taken into account in the mass estimate, the quasar’s intrinsic luminosity, and therefore its BH mass, will be overestimated. Previous considerations of the probability that these SDSS quasars are lensed indicate that while the a priori lensing probability is small, the magnification bias is poorly known and can be quite large (Wyithe & Loeb 2002). If massive BHs grow from stellar-mass seeds by accreting gas at the Eddington rate, they reach masses of $\sim 10^9 M_\odot$ in $\sim 10^9$ years, a time span comparable to the age of the universe at $z \sim 6$ in the current “best-fit” cosmologies.

Since the presence of such massive BHs can only be marginally accommodated into structure formation models (Haiman & Loeb 2001), it is interesting to ask whether *all* of the SDSS quasars may be strongly lensed. In this paper, we compute the expected probabilities for lensing of $z \sim 6$ quasars by intervening galaxies. We quantify how the probability depends on the shape of the assumed quasar LF, and in particular, we focus on the question: can the expected probabilities reach values near unity? We show that current constraints on the $z \sim 6$ quasar LF are sufficiently weak that the probabilities for strong lensing can indeed be close to 100%. We will utilize this result to “invert” the problem, and demonstrate how the intrinsic LF can be constrained using current and future detections (or absence) of lensing events with multiple images.

The rest of this paper is organized as follows. In § 2, we describe our model for the population of gravitational lenses. In § 3, we derive the resulting intrinsic “a priori” lensing probabilities along a random line of sight to redshift $z \sim 6$. In § 4, we discuss the effects of magnification bias, and the expected a posteriori lensing probabilities for the $z \sim 6$ quasars in models with different LFs. In § 5, we quantify constraints on the quasar LF that can be derived from current and future searches for lensing events. Finally, in § 6, we discuss our main results and then summarize the implications of this work. Throughout this paper, we adopt a flat cosmological model dominated by cold dark matter (CDM) and a cosmological constant (Λ), with $\Omega_m = 0.25$, $\Omega_b = 0.04$, and $\Omega_\Lambda = 0.75$, a Hubble constant $H_0 = 70 \text{ km s}^{-1}$, an rms mass fluctuation within a sphere of radius $8 h^{-1} \text{ Mpc}$ of $\sigma_8 = 0.9$, and power-law index $n = 1$ for the power spectrum of density fluctuations. We also adopt the cosmological transfer function from Eisenstein & Hu (1999).

¹ Hubble Fellow

2. MODEL DESCRIPTION

The a priori probability of gravitational lensing depends primarily on the comoving number density of lenses and the lensing cross section of each lens. Present theories agree that galaxies are created by the condensation of gas in dark matter halo cores, and the abundance of the most massive halos depends on the overall amplitude of mass fluctuations. We use the halo mass function of Jenkins et al. (2001), who measure dn/dM , the number of halos per unit comoving volume and per unit mass, from N -body simulations.

We employ a combination of two separate lens density profiles. The simpler of the two halo density profiles we consider is the singular isothermal sphere (SIS) density profile. The SIS profile is characterized by its dependence on the one-dimensional velocity dispersion, which is supported by observations of flat rotation curves, and its density profile is $\rho(r) = \sigma_v^2/2\pi Gr^2$, where σ_v is the velocity dispersion. The steep inner density slope of the SIS profile, however, renders it a poor fit to the more massive, and more extended halos. As a result, Navarro, Frenk, & White (1997; hereafter NFW) proposed a “universal” mass density profile for dark matter halos found in numerical simulations. The NFW density profile is $\rho(r) = \rho_s r_s^3/r(r+r_s)^2$, where ρ_s and r_s are constants. Although it matches the SIS model at intermediate radii, it branches off for large and small radii.

Because of the dynamics of cooling gas in halos (Keeton 1998; Porciani & Madau 2000; Kochanek & White 2001; Li & Ostriker 2002), we use a combination of the SIS and NFW profiles to describe the halos that contribute to the quasar lensing probability. Gas falling into very massive halos is shock-heated to high temperatures ($T \gtrsim 10^7\text{K}$) and cannot cool within a Hubble time. The gas therefore remains in hot, extended gaseous halos around groups or clusters of galaxies which have shallow inner density profiles. For less massive halos, in contrast, the virial temperature is low enough that the gas can cool and collapse into galaxies with steep inner density slopes. This difference in density slopes implies that a single density profile cannot describe all lensing objects in the universe.

As a solution, we use the SIS profile ($d\rho/dr \sim r^{-3}$) for less massive halos which have steep inner density slopes and the NFW profile ($d\rho/dr \sim r^{-2}$ for $r \ll r_s$) for more massive halos which have shallow inner density slopes. We set the transition between these two profiles at a dark matter halo mass of $10^{13}M_\odot$, the mass at which typically half of the dark halos have cooled the majority of their gas content, as given by the halo cooling probability distribution in Kochanek & White (2001). While this value of the cutoff has a physical basis, perhaps more importantly the predicted splitting angle distribution for lensing events with multiple images matches observations (Keeton 1998; Kochanek & White 2001; Li & Ostriker 2002). Therefore, in our calculations, we used the SIS profile for halo masses less than $10^{13} M_\odot$ and the NFW profile for halo masses greater than $10^{13} M_\odot$.

NFW halos are very inefficient lenses, with a cross-section per unit mass $\gtrsim 100$ times smaller than for SIS halos. Although the high mass halos are responsible for most lensing events with large ($\gtrsim 5''$) image splittings, these comprise only a small ($\sim 1\%$) fraction of all lensing

events of interest. As a result, in practice, we find that we can safely ignore NFW halos, and use a model where halos with masses below $10^{13} M_\odot$ are assumed to have SIS profiles, and halos with masses above $10^{13} M_\odot$ are simply excluded from the calculations. Our results for the intrinsic lensing probability are relatively insensitive to the choice of this mass cutoff: a factor of two higher/lower value would increase/decrease the intrinsic lensing probability to $z \sim 6$ by $\approx 20\%$. The effect on the a posteriori lensing probability is similar in models where the probability is relatively low ($\lesssim 50\%$), but the mass cutoff has a smaller effect on the a posteriori lensing probability if this probability is high (see discussion below).

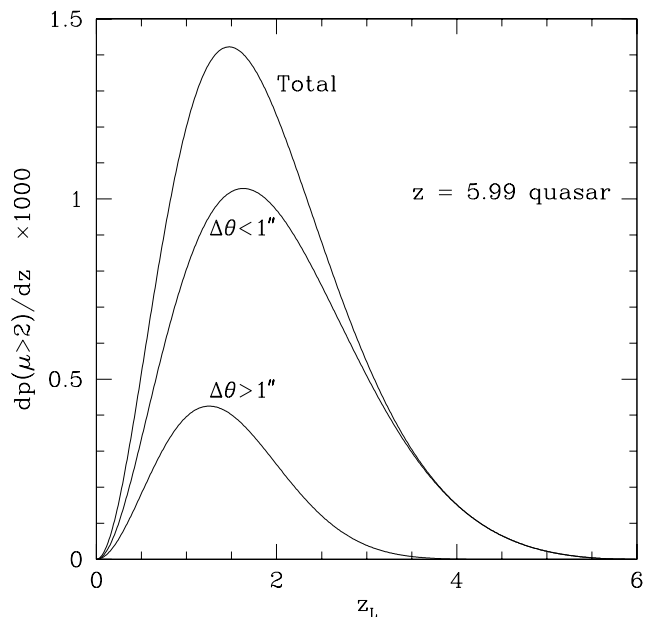


FIG. 1.— The a priori probability as a function of lens redshift that the $z = 5.99$ SDSS quasar was magnified by at least a factor $\mu_{\min} = 2$, but has not produced two separately detectable images for SDSS. The middle curve in the figure shows the probability for multiple images with an image splitting of $\Delta\theta < 1''$. The bottom curve shows the probability for image splittings of $\Delta\theta > 1''$, but subject to the constraint that the fainter image must be below the SDSS detection limit (this corresponds to $2 \leq \mu \leq 6.172$ for this source). The top curve shows the total lensing probability.

3. A PRIORI LENSING PROBABILITY

The a priori probability that a quasar is lensed by an intervening galaxy is given by the product of the number of lenses per unit volume, $(1+z)^3 dn/dM$, the galaxy lensing cross section, σ_L , and the path length of light from the quasar, $c(dt/dz) dz$, where $dt/dz = -1/(1+z)H(z)$, integrated over all possible lens masses M_L and redshifts z_L . Therefore, the a priori probability that a source at redshift z_s is lensed and magnified by a factor $\geq \mu$ is

$$p(\mu, z_s) = \int_0^\infty \int_0^{z_s} c \frac{(1+z_L)^2}{H(z_L)} \sigma_L(> \mu; M_L, z_L, z_s) \times \frac{dn}{dM}(M_L, z_L) dz_L dM_L, \quad (1)$$

where the Hubble parameter at redshift z in a flat universe is $H(z) = H_0[\Omega_m(1+z)^3 + \Omega_\Lambda]^{1/2}$, dn/dM is the

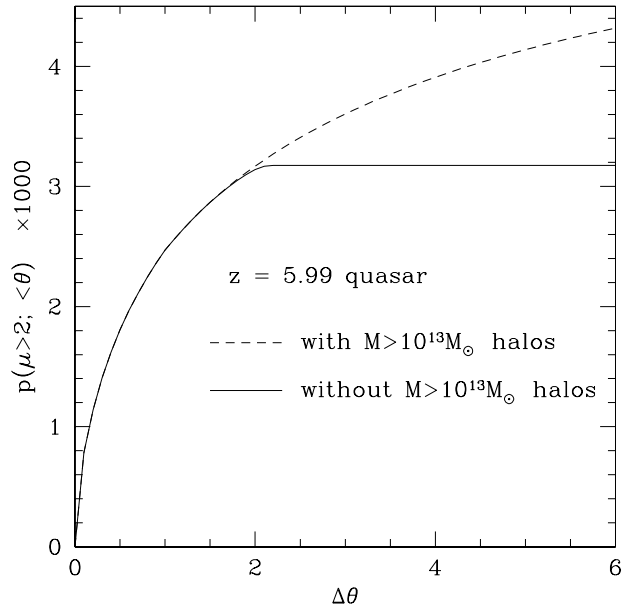


FIG. 2.— The a priori probability for the $z = 5.99$ SDSS quasar to be magnified by at least a factor of two, as a function of the maximum allowed splitting angle $\Delta\theta$. The dashed curve includes all halos, and assumes that each halo is described by an SIS profile. The solid curve excludes halos above $10^{13} M_{\odot}$. Including halos above this mass, described by NFW profiles, would yield a curve that is nearly identical to the solid curve. For splitting angles of $\Delta\theta > 1''$ we require that the fainter image must be below the SDSS detection threshold. This excludes lensing events with $\mu \geq 6.172$, and causes a $\sim 10\%$ decrease in the lensing probability for $\Delta\theta > 1''$.

comoving halo mass function from Jenkins (2001), and σ_L is the cumulative lensing cross-section in the lens plane for lensing amplification by a factor $> \mu$ by a SIS (see Schneider, Ehlers & Falco 1999). Note in particular that the cross section scales with the magnification as $\sigma_L \propto \mu^{-2}$ for $\mu > 2$, and as $\sigma_L \propto (\mu - 1)^{-2}$ for $\mu < 2$.

Fig. 1 shows the a priori probability $dp(\mu = 2, z_s = 5.99)/dz_L$ as a function of lens redshift that the $z = 5.99$ quasar SDSSp J130608.26+035636.3 (magnitude $z^* = 19.47$) was magnified by at least a factor $\mu_{\min} = 2$, but has not produced two images separately detectable by SDSS. The middle curve in the figure shows the lensing probability for multiple images with an image splitting of $\Delta\theta < 1''$, approximately the angular resolution of the SDSS (this corresponds to a redshift-dependent upper-mass cutoff of $\sim 10^{12} M_{\odot}$ for the lensing halos). The bottom curve shows the probability for image splittings of $\Delta\theta > 1''$, but subject to the constraint that the fainter image must be below the SDSS detection limit of $z^* = 20.2$. Note that for an SIS lens, multiple (i.e., two) images are formed for $\mu \geq 2$, with a flux ratio $\mu_1/\mu_2 = (\mu_{\text{tot}} + 2)/(\mu_{\text{tot}} - 2)$. Thus, the flux ratio is close to unity for high magnifications, and increases monotonically for lower total magnifications. In practice, the constraint that only one image be detectable simply imposes a maximum total magnification of $\mu_{\max} = 2(10^{0.4\Delta m} + 1)/(10^{0.4\Delta m} - 1)$. This source is $\Delta m = 0.73$ mag above the detection threshold and thus $\mu_{\max} \approx 6.172$. The top curve in Fig. 1 shows the total

lensing probability. As the figure shows, the total probability is very small, of order 0.1 percent, and reaches a maximum near a lens redshift of $z_L = 1.5$.

Fig. 2 illustrates how the total lensing probability, $p(\mu > 2, z_s = 5.99)$, depends on the maximum allowed image separation. For small splitting angles the probability increases steeply, whereas for large angular separations it flattens out. The dashed curve is for all halos, while the solid curve only includes halos less massive than $10^{13} M_{\odot}$. As discussed above, for the purposes of gravitational lensing, halos more massive than $10^{13} M_{\odot}$ are better described by NFW profiles, which have a much smaller cross-section for lensing than halos with SIS profiles. Including the $M > 10^{13} M_{\odot}$ halos using NFW profiles would result in a curve that is nearly identical to the solid curve. In both curves shown in this figure, for splitting angles of $\Delta\theta > 1''$, we require that the fainter image must be below the SDSS detection threshold. As discussed above, this excludes lensing events with $\mu \geq 6.172$, and causes a $\sim 10\%$ decrease in the lensing probability for $\Delta\theta > 1''$. Note that according to Figure 2, $\sim 75\%$ of all lensing events have image separations below $1''$, but only $\sim 10\%$ have image separations below $0.1''$.

Our results in this section agree to within a factor of two with previous estimates of the lensing probability and its dependence on lens redshift, e.g. by Kochanek (1998) and by Barkana & Loeb (2000). We conclude that the a priori lensing probability for a $z \sim 6$ SDSS quasar along a random line of sight is small, and dominated by lenses between redshifts $1 \lesssim z_L \lesssim 2$.

4. A POSTERIORI LENSING PROBABILITY

The a priori lensing probability calculated in §3 reflects the probability that lensing causes magnification by a factor of at least μ along a random line of sight. However, we are interested in the *a posteriori* probability that a given SDSS quasar has been lensed. Since the SDSS can only detect $z \sim 6$ quasars that are at the bright-end tail of the LF (if extrapolated from lower redshift), the magnification bias, defined as the ratio between the a posteriori and the a priori probability, could well be significant.

We determine the a posteriori lensing probability from the observed quasar LF. If we define $\Phi_{\text{int}}(L)$ as the intrinsic space density (assuming no lensing) of quasars with luminosity $L \pm dL/2$, then, given the intrinsic differential lensing probability $dp/d\mu$, the space density of quasars that will be observed at luminosity $L_{\text{obs}} \pm dL_{\text{obs}}/2$ and redshift z_s , and that are magnified by at least a factor μ_{\min} is

$$\Phi_{\text{obs}}(L_{\text{obs}}, \mu_{\min}) = \int_{\mu_{\min}}^{\infty} d\mu \frac{dp}{d\mu} \Phi_{\text{int}}(L_{\text{obs}}/\mu) \frac{1}{\mu}. \quad (2)$$

Similarly, the total space density of quasars observed at the same luminosity and redshift, regardless of their amplifications, is $\Phi_{\text{obs}}(L_{\text{obs}}, 0)$ and the a posteriori probability that a quasar with observed luminosity L_{obs} is lensed by a minimum factor μ_{\min} is

$$P(> \mu_{\min}) = \frac{\Phi_{\text{obs}}(L_{\text{obs}}, \mu_{\min})}{\Phi_{\text{obs}}(L_{\text{obs}}, 0)}. \quad (3)$$

The magnification bias and the a posteriori lensing probability depend strongly on the shape of the quasar LF. If the LF is steep or extends to faint luminosities, the magnification bias can be strong. Note that the magnification

bias depends only on the shape of the LF, not on its normalization. For the purpose of calculating $P(> \mu_{\min})$, we need, in principle, to extend the intrinsic lensing probability distribution to cover the full range of amplifications, including de-amplification, $0 < \mu < 2$. We shall use the following form of $dp/d\mu$:

$$\frac{dp}{d\mu} = \begin{cases} 8\tau_2/\mu^3 & (\mu \geq 2) \\ \tau_2/(\mu-1)^3 & (\mu_0 < \mu < 2) \\ \tau_2/(\mu_0-1)^3 & (1 \leq \mu < \mu_0) \\ 0 & (\mu < 1) \end{cases} \quad (4)$$

Here $\tau_2 = \int_2^\infty d\mu(dp/d\mu)$ is the total optical depth for forming double images (which depends on the source redshift, and is obtained from equation 1). The top two rows in equation (4) describe an SIS lens as usual, with a normalization that ensures a smooth transition from the case when the source is doubly imaged (but unresolved) to the singly imaged case. In order to correctly model the probability distribution near $\mu = 1$, we would have to allow for magnifications smaller than unity, which would require modeling the large-scale density distribution of the universe. Instead, we have imposed a critical magnification $\mu_0 \sim 1$, below which the probability is set to a constant. The value of μ_0 is chosen to be

$$\mu_0 = 1 + \sqrt{\frac{3\tau_2}{2 - \tau_2}}, \quad (5)$$

which enforces the normalization $\int_0^\infty d\mu \frac{dp}{d\mu} = 1$. Note that this simple characterization does not strictly conserve flux, since the mean magnification $\int_0^\infty d\mu \frac{dp}{d\mu} \mu > 1$. However, in practice, we find that μ_0 and the mean magnification are close to unity, and our results are insensitive to our treatment of $dp/d\mu$ near $\mu = 1$.

To calculate the a posteriori lensing probability of the high redshift SDSS quasars, we also need to know their intrinsic LF. We here assume that the intrinsic $z \sim 6$ quasar LF can be described by the double power law form given in Pei (1995):

$$\Phi_{\text{int}}(L) = \frac{\Phi_*/L_*}{(L/L_*)^{\beta_l} + (L/L_*)^{\beta_h}}. \quad (6)$$

The same form was used by Madau, Haardt, & Rees (1999) and more recently by Wyithe & Loeb (2002), with different sets of parameters. The LF depends on four parameters: the normalization Φ_* , the faint-end slope β_l , the bright-end slope β_h , and the characteristic luminosity L_* at which the LF steepens. The a posteriori lensing probability is sensitive to the last two parameters, β_h and L_* (and is strictly independent of the normalization Φ_*).

Through different combinations of slopes and breaks, we present seven possible LFs at redshift $z = 6$, which are illustrated in Fig. 3. All models have $\beta_l = 1.64$ (Pei 1995) and the normalization Φ_* has been adjusted so that each curve passes through the Fan et al. (2001b) data point corresponding to the space density implied by the four $z \sim 6$ quasars. The curves in the upper panel all have $\beta_h \approx 3.5$, but L_* varies from $\approx 10^{10} L_{B,\odot}$ for the Pei (1995) model (solid curve) to $\approx 10^{12} L_{B,\odot}$ for the model of Madau et al. (1999). The curves in the bottom panel all have $L_* \approx 10^{11.5} L_{B,\odot}$, but have different values of β_h . The parameters of the LFs are summarized in Table 1.

TABLE 1
PARAMETERS OF THE $z = 6$ QUASAR LUMINOSITY FUNCTIONS.

| | $\log(\frac{L_*}{L_{B,\odot}})$ | $\log(\frac{\Phi_*}{L_{B,\odot}^{-1} \text{Gpc}^{-1}})$ | β_l | β_h |
|--------------------------|---------------------------------|---|-----------|-----------|
| Varying Break | | | | |
| Pei (1995) | 10.10 | 6.57 | 1.64 | 3.52 |
| Pei (1995) ² | 10.87 | 4.61 | 1.64 | 3.52 |
| WL (2002) | 11.95 | 1.91 | 1.64 | 3.52 |
| MHR (1999) | 11.55 | 2.76 | 1.64 | 3.43 |
| Varying Bright End Slope | | | | |
| steep | 11.55 | 4.63 | 1.64 | 4.5 |
| medium | 11.55 | 2.88 | 1.64 | 3.5 |
| shallow | 11.55 | 1.14 | 1.64 | 2.5 |

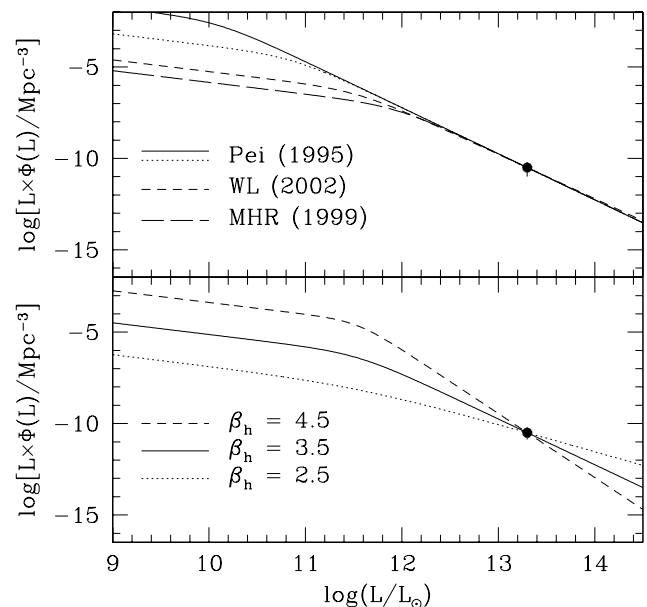


FIG. 3.— The seven different LFs used to compute lensing probabilities. The LFs are all described by a double power law with the same faint-end slope of $\beta_l = 1.64$, and are shown at redshift $z = 6$. The data point is from Fan et al. (2001) and represents the space density of luminous quasars at $z \approx 6$, inferred from the discovery of the four SDSS quasars ($\log(L\Phi/\text{Mpc}^{-3}) = -10.5$ at $\log(L_B/L_{B,\odot}) = 13.3$). The *upper panel* demonstrates the effect of varying the break of the LF. From top to bottom the four LFs have $\log(L_*/L_{B,\odot}) \approx 10.1, 10.9, 11.5,$ and 11.9 respectively. Apart from the normalization Φ_* , which has been adjusted to ensure consistency with the SDSS data point, the curves correspond to the model of Pei (1995) (solid), the Pei (1995) model with a 6 times larger L_* (dotted), the model of Wyithe & Loeb (2002) (short dashed), and Madau et al. (1999) model (long dashed). The Wyithe & Loeb (2002) model (short dashed) has $\beta_h = 3.43$, while the other models have $\beta_h = 3.52$. The *lower panel* demonstrates the effect of varying the bright-end slope β_h from 2.5 to 4.5. All three models have $\log(L_*/L_{B,\odot}) \approx 11.5$. See Table 1 for a summary of the LF parameters.

The values are given at redshift $z = 6$; we allow for slightly different values for the characteristic luminosity over the range $5.8 < z < 6.28$ by including the redshift dependence of L_* as parameterized in each case by Pei (1995), Madau

et al. (1999), and Wyithe & Loeb (2002).

The lensing probability depends on the intrinsic LF, which is not directly observable. In using the Fan et al. (2001b) data point as a constraint on the intrinsic LF, we thus implicitly assumed that lensing does not have a large overall effect on the LF. If magnification bias is significant, then this assumption breaks down for the bright-end of the LF. Thus, to match the observations, the normalizations of the intrinsic LFs should in fact be lowered by a factor equal to the magnification bias for the observed quasars. However, for the purpose of computing the a posteriori lensing probability this is irrelevant, since the magnification bias is independent of the normalization of the intrinsic LF.

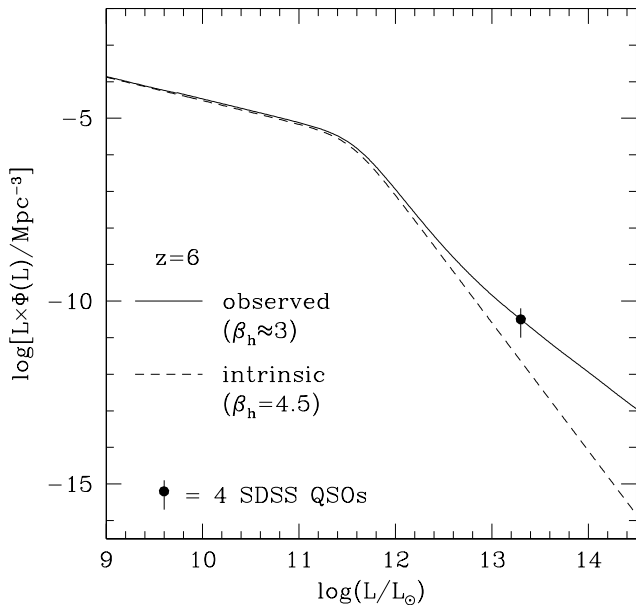


FIG. 4.— A comparison of the intrinsic and observed LFs for our most extreme model, which has an intrinsic bright-end slope of $\beta_h = 4.5$ (see dashed curve in lower panel of Fig. 3). The lensing probability at $z = 6$ in this case is high, and the apparent LF is increased by over an order of magnitude at the luminosity of the SDSS quasars. The apparent slope is flattened to $\beta \approx 3$, and the model is therefore consistent with the upper limit on slope of the apparent LF from the SDSS ($\beta < 4.3$ at 99 percent confidence, Fan et al. 2001).

The SDSS observations provide an upper limit on the slope of the bright-end of the observed LF: $\beta_{h,obs} < 4.3$ at 99 percent confidence (Fan et al. 2001a,b). If magnification bias is important, then this constraint will always be satisfied since lensing by an isothermal sphere will result in a bright-end slope of $\beta_{h,obs} = 3.0$ (the intrinsic differential lensing probability $dp/d\mu \propto \mu^{-3}$ for $\mu > 2$). This is illustrated in Fig. 4, which shows the intrinsic and observed LFs for our most extreme model, which has $\beta_h = 4.5$ (dashed curve in the lower panel of Fig. 3). Since the magnification bias increases with β_h , observations cannot directly constrain the steepness of the intrinsic, bright-end slope of the LF. However, we will see below that the slope can be constrained indirectly, by measuring the fraction of multiply imaged quasars.

Fig. 5 shows the a posteriori probabilities for the $z =$

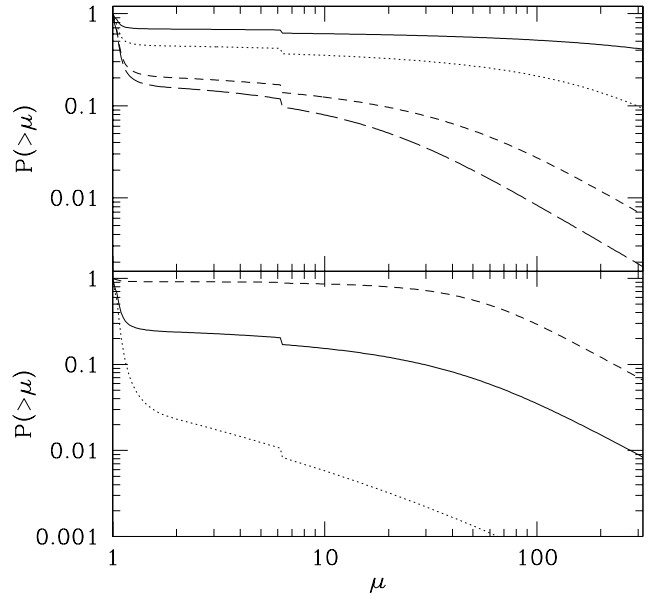


FIG. 5.— Lensing probability as a function of minimum magnification μ for the $z = 5.99$ SDSS quasar and the seven different LFs shown in Fig. 3. Note that the total lensing probability is sensitive to variations of both the slope β_h and break L_* , and can be high. For $\mu > 6.172$, both lensed images would appear brighter than SDSS's threshold, and we impose the condition $\Delta\theta < 1''$ on their splitting angle to avoid detection by SDSS. On the other hand, the fainter image is too faint to be detectable, and we allow lensing with arbitrarily large splitting angles for $\mu < 6.172$.

5.99 SDSS quasar to be magnified by at least a factor μ , subject to the constraint that only one image is detectable by SDSS. The small discontinuity in the probabilities at $\mu = 6.172$ occurs because for $\mu < 6.172$ the fainter image is too faint to be detectable, and we do not impose any constraint on the splitting angle. On the other hand, for $\mu > 6.172$ both images would be brighter than SDSS's threshold, and we therefore impose the condition $\Delta\theta < 1''$ on the splitting angle. The seven curves shown in Fig. 5 correspond to the seven intrinsic LFs in Fig. 3. From the figure it is clear that a wide range of probabilities is possible for a given minimum magnification. In particular, because of the lack of constraints on the intrinsic LF, they can be significantly higher than the maximum value of $\sim 30\%$ found by Wyithe & Loeb (2002), who considered a more restricted range of LFs (the short dashed curve in the upper panel in Fig. 3 represents their most extreme model that results in their maximum lensing probabilities). For example, if L_* is small, as for the Pei (1995) model (solid curve in upper panel), then the probability that the quasar has been magnified by more than a factor of ten is about sixty percent. The lensing probability also becomes very large if the bright-end slope is steep: $P(\mu > 10)$ is close to unity if $\beta_h = 4.5$ (dashed curve in the lower panel). In Table 2, in the last line, we list the lensing probability for each of the four quasars in this model.

TABLE 2
PARAMETERS AND LENSING PROBABILITIES OF THE FOUR $z \approx 6$ SDSS QUASARS^a

| | 1044-0125 | 0836-0054 | 1306-0356 | 1030-0524 |
|---|-----------|-----------|-----------|-----------|
| Redshift | 5.80 | 5.82 | 5.99 | 6.28 |
| Magnitude [z^*] | 19.23 | 18.74 | 19.47 | 20.05 |
| τ_2 [any $\Delta\theta$] | 0.00314 | 0.00315 | 0.00326 | 0.00344 |
| τ_2 [$\Delta\theta < 1''$] | 0.00238 | 0.00239 | 0.00247 | 0.00260 |
| μ_{\min} | 4.771 | 3.410 | 6.172 | 28.99 |
| $P(\mu > \mu_{\min})$ [$\Delta\theta > 1'', \beta_h = 4.5$] | 0.220 | 0.231 | 0.218 | 0.150 |
| $P(\mu > 10)$ [$\Delta\theta < 1'', \beta_h = 4.5$] | 0.877 | 0.939 | 0.862 | 0.788 |

^aThe first two lines list the redshift and magnitude of each source. The 3rd and 4th lines give the optical depth to lensing with amplification $\mu \geq 2$ with and without including events whose splitting angles are larger than $1''$. The 5th line lists the minimum total magnification for which both images are above the SDSS magnitude threshold of $z^* = 20.2$. The last two lines list the lensing probabilities, with magnification bias taken into account, in our most extreme model with a bright-end quasar LF slope of $\beta_h = 4.5$. The 6th line gives the probability for an event that produces two separately detectable images for SDSS. The last line gives the probability for an unresolved lensing event with total magnification $\mu \geq 10$.

5. CONSTRAINING THE SHAPE OF THE LUMINOSITY FUNCTION

In the previous section we have demonstrated that it is possible that most of the $z \sim 6$ SDSS quasars are strongly magnified by gravitational lensing, and that the expected lensing probability depends very strongly on the shape of the intrinsic quasar LF. Because of the unknown magnification bias, surveys that probe only the bright-end of the LF ($L > L_*$), cannot directly measure the intrinsic LF. However, it is possible to constrain the intrinsic LF, in particular the characteristic luminosity L_* and the bright-end slope β_h , by measuring the fraction of multiply imaged quasars down to a fixed limiting angular resolution.

The SDSS survey has so far discovered four $z \sim 6$ quasars (Fan et al. 2001), all of which appear to be single images at the angular resolution ($\sim 1''$) and detection limit ($z^* = 20.2$) of the survey. The parameters of these quasars are listed in Table 2. Lensing by an isothermal sphere always yields a double image if the total magnification is greater than two. Thus, if these object are strongly lensed, then the extra image must have escaped attention either because the splitting angle was too small for SDSS to resolve the images or because one of the images was too faint to be detected. In the previous section, when we computed the a posteriori probabilities for lensing, we took these limitations of the survey into account.

In this section, we relax these limitations, and compute the complementary quantity: the probability of lensing events that would produce multiple images, both of which would have been detectable by SDSS (i.e., we require that both images be above the detection threshold, and separated by $> 1''$). The lack of such a detection can be used to constrain models for the LF. In particular, for a given quasar LF, we can compute the likelihood that *at least one* of the four SDSS quasars would exhibit two images. This is given by $P = 1 - (1 - P_1) \times (1 - P_2) \times (1 - P_3) \times (1 - P_4)$, where P_i is the probability for the i^{th} quasar to be doubly imaged. We consider variations in the two parameters L_* and β_h of the quasar LF, and compute P as a function of L_* and β_h . As an example, in Table 2, in the 6th line, we list the probability for each quasar to be doubly imaged in our most extreme model for the quasar LF.

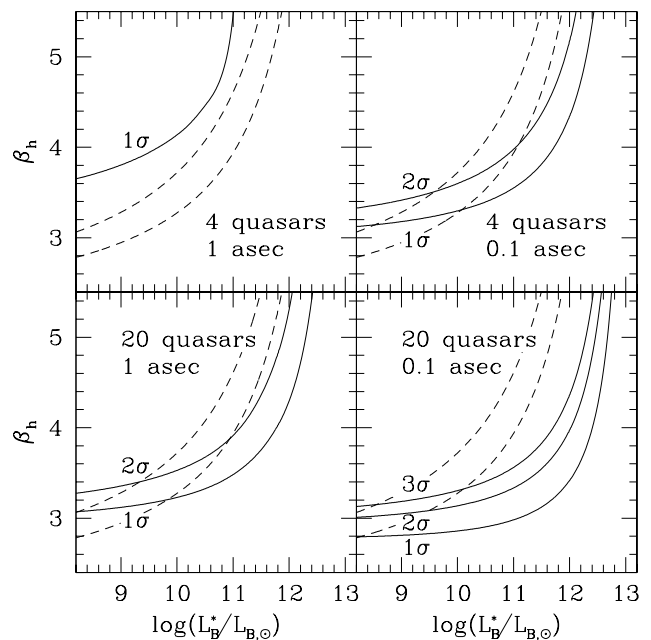


FIG. 6.— Constraints on the parameters of the redshift $z = 6$ quasar LF from the non-detection of gravitational lenses. The solid curves show likelihood contours for ruling out a given LF, if no gravitational lenses are found. The upper left panel shows the 1σ constraint from the existing four SDSS quasars, assuming that double images are resolvable if they are separated by $> 1''$, and are both above the magnitude threshold of $z^* = 20.2$. The constraint is weak. The other three panels demonstrate how the constraint can be improved if no lenses are found despite (i) increasing the angular resolution to $0.1''$ (upper right panel); (ii) increasing the sample size to a total of 20 quasars (lower left panel); or (iii) both (lower right panel). The 3σ contour is off the scale of the plots, except in the lower right panel; the 2σ contour is off the scale in the upper left panel. The dashed curves show contours of fixed ionizing background $\Gamma_{-12} = 0.1$ and $\Gamma_{-12} = 2$.

In the upper left panel of Fig. 6, we show the constraint on the intrinsic LF resulting from the non-detection of any multiple images in the four quasars reported in Fan et al. (2001). The solid curve corresponds to the constant $P = 0.68$, i.e., models that lie above the solid curve are excluded

at the 1σ level. The analogous 2 and 3σ contours are off the scale of the plot. The SDSS observations do not yet place strong constraints on the intrinsic LF. This can be understood as follows: the intrinsic probability for lensing with multiple images to $z = 6$ when all lensing halos are considered (up to a mass $10^{13} M_{\odot}$, see § 3) is $\tau_2 = 0.00326$, but when splittings of $> 1''$ are excluded, the probability is $\tau_2 = 0.00247$. In other words, only $\sim 25\%$ of all lensing events would be resolved at $> 1''$. Even for an arbitrarily large magnification bias, SDSS would only have a $\sim 25\%$ chance of resolving the multiple images of a given quasar (see Table 2). Note that the $z = 6.28$ source is very close to the SDSS magnitude threshold, and the fainter image would escape detection unless the total magnification is $\mu > 29$. As a result, the probability for producing an additional detectable image for this source is smaller than for the other three quasars.

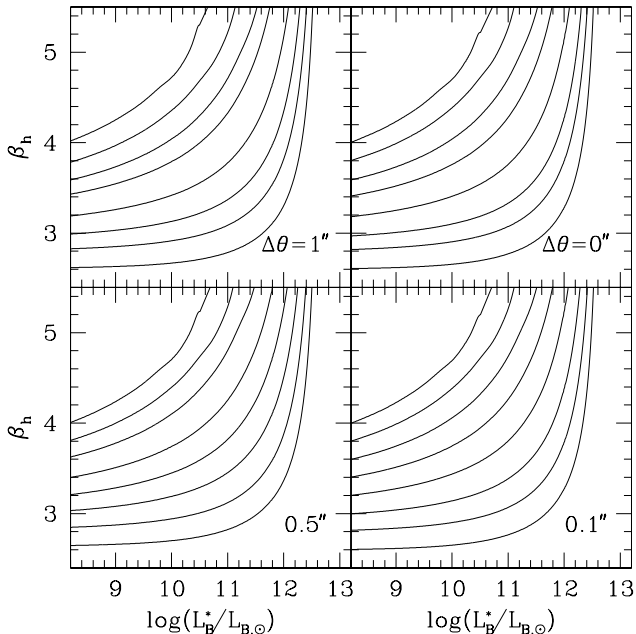


FIG. 7.— Likelihood contours as in Fig. 6, but for a single $z = 6$, $z^* = 20$ quasar. The curves in each of the four panels show constant probabilities for a lensing event that is detectable at different angular resolutions (the upper right panel assumes infinite resolution, i.e., it includes all multiple lensing events). Each panel shows 8 curves, corresponding to the following probabilities (bottom to top, in percent): (i) Upper left panel: 1, 2, 4, 10, 20, 23, 24, 24.18; (i) Upper right panel: 4, 8, 15, 40, 80, 95, 99.3, 99.9; (i) Lower left panel: 2, 4, 9, 20, 35, 43, 44.3, 44.55; (i) Lower right panel: 3, 6, 13, 33, 60, 72.5, 75.4, 75.86. Note the “saturation” of the probabilities near the top contour in each panel, caused by the finite fraction of lensing events that produce splittings above a given angular resolution.

In the remaining three panels of Fig. 7 we illustrate how future observations would constrain the LF if no multiple images were detected. The bottom left panel shows the results for 20 objects with properties identical² to the four already discovered quasars. If SDSS were to discover 20 $z \sim 6$ quasars, and none of them showed a second image,

² In increasing the sample size, we simply replicated the current sample of quasars five times. Since the lensing probabilities are similar for quasars near the detection threshold and near $z = 6$, our results are not sensitive to this particular choice.

then the more extreme intrinsic LFs plotted in Fig. 3 (the Pei 1995 and the $\beta_h = 4.5$ models) would be ruled out at the 2σ level.

The upper right panel shows that nearly identical constraints can be obtained by observing the four already known quasars with an angular resolution of $0.1''$, a resolution typical for observations with the *Hubble Space Telescope* (for the cases of a maximum splitting angle of $0.1''$ we assumed that sufficient depth is reached that both images are detectable, and did not impose a magnitude cut, or a constraint on the flux ratio). Finally, the bottom right panel shows that observations of 20 quasars at $0.1''$ resolution would enable us to put very strong constraints on the intrinsic LF, with the current “ball-park” LFs, obtained by extrapolations from lower redshifts, ruled out at the $\sim 3\sigma$ level.

In these examples we assumed that no multiple images are detected. Similar calculations can of course be done if future observations would detect one or more multiple images. In that case the likelihood contours can be closed and the parameters of the LF would be constrained both from above and from below. To enable interpretation of any outcome of a future search for lenses, Figure 7 shows probability contours for multiple lensing for a single $z = 6$, $z^* = 20$ quasar. The curves in each of the four panels show constant probabilities for a lensing event detectable at four different angular resolutions (the upper right panel assumes infinite resolution, i.e., it includes all multiple lensing events). Each panel shows 8 curves, corresponding to the following probabilities (bottom to top, in percent): (i) Upper left panel: 1, 2, 4, 10, 20, 23, 24, 24.18; (i) Upper right panel: 4, 8, 15, 40, 80, 95, 99.3, 99.9; (i) Lower left panel: 2, 4, 9, 20, 35, 43, 44.3, 44.55; (i) Lower right panel: 3, 6, 13, 33, 60, 72.5, 75.4, 75.86. Note the “saturation” of the probabilities near the top contour in each panel, caused by the finite fraction of lensing events that produce splittings above a given angular resolution.

Varying the intrinsic LF does not only affect the lensing probability, but also changes the total amount of emitted quasar light, including the ionizing emissivity. Since the ionizing background can in principle be measured, this can provide an additional constraint on the quasar LF. Observations of the mean absorption in the Lyman- α forest have been used recently to infer the ionizing background at $z \sim 6$ (Becker et al. 2001; Cen & McDonald 2001; McDonald & Miralda-Escudé 2001; Fan et al. 2002), yielding ionization rates per hydrogen atom of $\Gamma_{-12} \equiv \Gamma/10^{-12}\text{s}^{-1} \approx 0.1$. The dashed curves in Fig. 6 show contours of fixed quasar emissivity, corresponding to $\Gamma_{-12} = 0.1$ and 2 respectively. Our method for computing the ionization rate from the LF is described in more detail in the Appendix below. At face value, LFs that lie above the lower dashed curve over-produce the ionizing background; those above the upper dashed curve by a factor of > 20 . However, in practice this result has large uncertainties. First, although the adopted quasar LF yields the total ionizing emissivity, the prediction of the ionizing background involves the mean free path of ionizing photons, which is highly uncertain at the redshifts of interest here. A small mean free path would reduce the background. Second, a smaller fraction of ionizing photons might escape from the dense surroundings of high-redshift quasars than

from their lower-redshift counterparts.

6. DISCUSSION AND CONCLUSIONS

In this paper, we computed the expected lensing probabilities of $z \sim 6$ quasars by intervening galaxies. The a posteriori probability that a $z \sim 6$ quasar is strongly lensed (by a factor $\mu > 10$ in flux enhancement), but without producing two images detectable in the Sloan Survey, can be very large, depending on the shape of the LF. The LFs we use are consistent with other available observational constraints, yet these constraints still allow for a wide range of possibilities.

Though an *observed* bright-end slope of $\beta_h = 4.3$ could be ruled out at the 99 percent confidence level (Fan et al. (2001)), lensing alters the slope so that the apparent LF will have a slope close to ~ 3.0 if magnification bias is important. As illustrated in Fig. 4, even the steepest intrinsic LF we consider, with a bright end slope of 4.5, is consistent with the SDSS limit on slope. This will be true for arbitrarily steep slopes, provided that the characteristic luminosity is not increased.

In a similar probability calculation, Wyithe & Loeb (2002) concluded that the observed probability reaches 30% that a single $z \sim 6$ quasar is lensed and magnified by a factor of 10 or more. If we restrict our analysis to the choices of LFs considered in their paper, we agree with this result. However, we here use a wider range of quasar LFs and conclude that the lensing probability can reach essentially 100%. As a result, the current observations are consistent with all four $z \sim 6$ SDSS quasars being strongly lensed.

If the probability that all four quasars are lensed were high, then this would alleviate the problematic time constraints on assembling supermassive black holes at the earliest stages in the evolution of the universe. However, in a separate analysis, based on the apparently large size of the ionized region around the SDSS quasar at $z = 6.28$, Haiman & Cen (2002) place a strong constraint on the lensing magnification of this source, and find $\mu < 5$. This result depends primarily on the assumption that the source is embedded in a neutral (rather than ionized) intergalactic medium.

We have also considered the probabilities for lensing events that would have been detectable by SDSS. The lack of such detections can be used to place constraints on the quasar LF. Although constraints from the current four quasars are mild, the situation is likely to improve. As illustrated in Fig. 6, increasing the SDSS sample from 4 to 20 objects, something that is likely to happen over the next few years, would allow one to rule out interesting quasar LF models. The expected probability of detecting multiple images is also sensitive to the angular resolution of the observations. In terms of the constraints on the shape of the intrinsic LF, observing four quasars at a resolution of $0.1''$ is roughly equivalent to observing 20 objects at the resolution of the SDSS ($1''$).

Hence, upcoming observations, in particular with the *Hubble Space Telescope*, should reveal whether a significant fraction of the $z \sim 6$ quasars is lensed, and will allow us to place strong constraints on their intrinsic LF.

We thank Michael Strauss and Xiaohui Fan for many

useful discussions. The work presented here is based on the senior thesis of JC at Princeton University. She thanks Neta Bahcall for her encouragement and advice. This work was supported by NASA through the Hubble Fellowship grant HF-01119.01-99A, awarded to ZH by the Space Telescope Science Institute, which is operated by the Association of Universities for Research in Astronomy, Inc., for NASA under contract NAS 5-26555. JS acknowledges support from the W. M. Keck foundation.

APPENDIX

Here we discuss constraints on the high-redshift quasar LF from their integrated ionizing radiation. Given an LF, we compute the total comoving emissivity as $\nu\epsilon_\nu = \int L\Phi(L)dL$. This gives $\nu\epsilon_\nu$ at rest-frame 4400 Å; however, with a spectral slope of $\epsilon_\nu \propto \nu^{-1}$ this is independent of wavelength, and has the same value at 912 Å. The background ionization rate per hydrogen atom Γ is then given by

$$\Gamma = \frac{\pi\sigma_H}{h_P} \lambda_{\text{mfp}} \frac{(1+z)^3 \nu\epsilon_\nu}{4\pi \nu_H} \text{ s}^{-1}, \quad (7)$$

where we have assumed $\epsilon_\nu \propto \nu^{-1}$, $\sigma_H = 6.3 \times 10^{-18} \text{ cm}^{-2}$ is the hydrogen ionization cross section at the Lyman limit (and we assumed $\sigma_H(\nu) \propto \nu^{-3}$ above the threshold), h_P is the Planck constant, $\nu_H = 3.29 \times 10^{15} \text{ Hz}$ is the frequency of a Lyman limit photon, and λ_{mfp} is the mean free path of ionizing photons. We also define $\Gamma_{-12} = \Gamma/10^{-12} \text{ s}^{-1}$. We assume that the effective mean free path corresponds to a redshift interval of $\Delta z = 0.17$ at $z = 3$ (see Haardt & Madau 1996 and Steidel, Pettini & Adelberger 2001), and scales with redshift as $\lambda_{\text{mfp}} \propto (1+z)^{-6}$ towards higher redshift (Cen & McDonald 2002). Based on recent measurements (e.g. Cen & McDonald 2002, see also Becker et al. 2001; McDonald & Miralda-Escudé 2001 and Fan et al. 2002), we require $\Gamma_{-12} < 0.1 \text{ s}^{-1}$ at $z=6$. We find that in some of our models, at $z = 6$, this bound is violated by up to a factor of 13: $\Gamma_{-12} = 1.3$ (Pei LF); $\Gamma_{-12} = 0.39$ (WL LF with a bright-end slope of $\beta_h = 4.5$); $\Gamma_{-12} = 0.08$ (Pei LF with 6 times higher L_*). More generally, contours of constant $\Gamma_{-12} = 0.1$ and $\Gamma_{-12} = 2$ are shown in Figure 6.

The apparently large ionizing emissivities imply that in our LF with the lowest L_* , the background is overproduced, although this result is subject to several uncertainties: (1) the escape fraction of ionizing photons may be only $\sim 10\%$ at $z = 6$; (2) the mean free path evolves more steeply than $(1+z)^{-6}$; (3) the faint-end slope is considerably shallower than $\beta_l = 1.64$, or (4) there can be significant systematic errors on the observational determination of Γ_{-12} , since it relies on cosmological simulations for modeling the temperature and density field.

REFERENCES

- Barkana, R., & Loeb, A. 2000, ApJ, 531, 613
- Becker, R. H., et al. 2001, AJ, 122, 2850
- Cen, R., & McDonald, P. 2001, ApJ, submitted, astro-ph/0110306
- Eisenstein, D. J., & Hu, W. 1999, ApJ, 511, 5
- Fan, X., et al. 2001a, AJ, 121, 54
- Fan, X., et al. 2001b, AJ, 122, 2833
- Fan, X., et al. 2002, AJ, 123, 1247

- Haardt, F. & Madau, P. 1996, *ApJ*, 461, 20
- Haiman, Z., & Cen, R. 2002, *ApJL*, submitted, astro-ph/0205143
- Haiman, Z., & Loeb, A. 2001, *ApJ*, 552, 459
- Jenkins, A., Frenk, C. S., White, S. D. M., Colberg, J. M., Cole, S., Evrard, A. E., Couchman, H. M. P., & Yoshida, N. 2001, *MNRAS*, 321, 372
- Keeton, C. R. 1998, Ph.D. thesis, Harvard Univ.
- Kochanek, C. S. 1998, in *Science with the NGST*, ed. E. P. Smith & A. Koratkar, ASP Conference Series vol. 133, p. 96
- Kochanek, C. S., & White, M. 2001, *ApJ*, 559, 531
- Li, L., & Ostriker, J. P. 2002, *ApJ*, 566, 652
- Madau, P., Haardt, F., & Rees, M. J. 1999, *ApJ*, 514, 648
- McDonald, P., & Miralda-Escudé, J. 2001, *ApJ*, 549, 11L
- Navarro, J. F., Frenk, C. S., & White, S. D. M. 1997, *ApJ*, 490, 493
- Pei, Y. C. 1995, *ApJ*, 438, 623
- Porciani, C., & Madau, P. 2000, *ApJ*, 532, 679
- Schneider, P., Ehlers, J., & Falco, E. E. 1999, *Gravitational Lenses* (Berlin: Springer), p. 386
- Steidel, C. C., Pettini, M., & Adelberger, K. L. 2001, *ApJ*, 546, 665
- Wyithe, S., & Loeb, A. 2002, *ApJ*, in press, astro-ph/0203119